Tissue Accumulation of Neutrophil Extracellular Traps Mediates Muscle Hyperalgesia in a Mouse Model

Kazuaki Suzuki
Tohoku University: Tohoku Daigaku https://orcid.org/0000-0001-7126-3420
Masahiro Tsuchiya (tsuchiya-thk@umin.ac.jp)
Department of Nursing, Tohoku Fukushi University, Sendai, Miyagi, Japan https://orcid.org/0000-0002-7000-4547
Shinichiro Yoshida
Tohoku University: Tohoku Daigaku
Kazumi Ogawa
Tohoku University: Tohoku Daigaku
Weijian Chen
Tohoku University: Tohoku Daigaku
Makoto Kanzaki
Tohoku University: Tohoku Daigaku
Tadahisa Takahashi
Tohoku University: Tohoku Daigaku
Ryo Fujita
Tohoku University: Tohoku Daigaku
Yuqing Li
Tohoku University: Tohoku Daigaku
Yutaka Yabe
Tohoku University: Tohoku Daigaku
Toshimi Aizawa
Tohoku University: Tohoku Daigaku
Yoshihiro Hagiwara
Tohoku University: Tohoku Daigaku

Research

Keywords: neutrophil extracellular trap, uric acid, muscle pain, citrullinated histone H3, multiphoton microscopy imaging

Posted Date: June 12th, 2021

DOI: https://doi.org/10.21203/rs.3.rs-576628/v1

Abstract

Background: Accumulation of uric acid during muscular trauma is potentially a causative factor of damage-associated molecular patterns (DAMPs) involved in the development of muscle hyperalgesia. Neutrophil extracellular traps (NETs), DNA-based reticular structures to capture DAMPs, play a central role in the onset of pain in gout attacks associated with hyperuricemia; however, their association with muscle hyperalgesia due to overuse injuries remains unknown. Therefore, the aim of this study was to investigate the involvement of NETs via the elevation of local uric acid level in muscle nociception.

Methods: The triceps surae muscles (TSMs) in the unilateral hindlimb of mice were repeatedly stimulated with electrical pulses to induce excessive muscle contraction, and the contralateral TSM was used as a control. In addition to mechanical nociceptive thresholds, tissue uric acid levels, neutrophil recruitment, protein amount, and histological distribution of citrullinated histone 3 (citH3), a major marker of NETs, were investigated. Furthermore, whether neutrophil depletion, extracellular DNA cleavage (deoxyribonuclease I), and administration of the urate-lowering agent febuxostat, a xanthine oxidase inhibitor, improved muscle hyperalgesia due to NET accumulation was examined. Using a combination of multiphoton imaging analysis and intravital fluorescence staining, we also evaluated the intramuscular distribution of NET accumulation in stimulated TSMs.

Results: CitH3 expression upon neutrophil recruitment significantly increased in the stimulated TSMs tissues with an increase in tissue uric acid levels. However, neutrophil depletion and extracellular DNA cleavage prevented the increase in uric acid levels in damaged muscle tissues. Furthermore, febuxostat administration significantly improved muscle hyperalgesia, with decreases not only in citH3 and tissue uric acid levels, but also in neutrophil recruitment. Interestingly, the intramuscular distribution of NETs in the stimulated TSM was predominantly observed in the myofascial region.

Conclusions: Our findings suggest that NET accumulation caused by excessive muscle contraction was strongly associated with the pathogenesis of muscle hyperalgesia. Further, the mechanism underlying induction of locally recruited neutrophils forming NETs was increased tissue uric acid levels, which potentially plays a significant role in creating a vicious circle of muscle pain.

Background

Skeletal muscle is a common source of pain that markedly impairs activities of daily living [1]. It is widely observed as a major sign of various pathologies, such as neck and shoulder pain [2], nonspecific lower back pain [3], and myofascial pain syndrome (MPS) [4]. Based on the higher lifetime prevalence of skeletal muscle pain among the labor population [5, 6], muscle overuse is a key pathogenic event in developing muscle pain. Fundamentally, overuse trauma prompts muscle fibers to release extracellular adenosine triphosphate (ATP), which directly activates pain signaling through purinergic and metabotropic receptors via autocrine and paracrine functions [7-10]. Indeed, both the serum and muscle

tissue levels of uric acid, an end product of purine nucleotides including ATP and dead cell DNA, are reportedly increased due to the production of damaged muscle fibers [11-15].

Uric acid has recently been recognized as a damage-associated molecular pattern (DAMP), which activates an intracellular complex called the inflammasome for processing and releasing interleukin (IL)-1β and IL-18 [16]. Our recent study using a muscle pain model by the repeated electrical stimulation of the triceps surae muscles (TSMs) revealed the marked recruitment of inflammatory cells, including neutrophils and macrophages, producing proinflammatory cytokines, such as IL-1β and IL-18; this was due to inflammasome activation, which was triggered by the increase in tissue uric acid levels [11, 15, 17]. Furthermore, based on the improvement of muscle hyperalgesia by the administration of xanthine oxidase inhibitors, we suggested that a higher tissue uric acid concentration could be a causative factor of mechanical hyperalgesia [11]. Thus, the dysregulated innate immune response with hyperuricemia has been associated with gout among various autoinflammatory diseases; these autoinflammatory diseases are characterized by unprovoked episodes of recurrent or continuous inflammation in the absence of high-titer autoantibodies or antigen-specific lymphocytes [18-20].

A recent study has also supported that the dysregulated innate immune response of neutrophils against monosodium urate (MSU) crystals in the gout flare is a part of the autoinflammatory response because of the involvement of neutrophil extracellular traps (NETs) [21]. The release of NETs, a unique defense mechanism continuing from cell death (NETosis), is regarded as a valuable target for disease pathogenesis in gout [21-23]. NETs are primarily composed of their own DNA released as reticular structures with an oxidative burst in order to capture and eliminate pathogens, including DAMPs [22, 23], and citrullinated histone H3 (citH3) plays a central role in NETosis. Interestingly, NETs also contribute to aggregating neutrophilic proinflammatory mediators, thereby limiting, but prolonging the inflammatory status [22]. Indeed, NETs are not only a DAMP after degradation, but also a potential source of uric acid with extracellular nucleotide metabolism [23]. Thus, research findings regarding the underlying mechanism of uric acid accumulation with a focus on NETs in damaged muscle tissues will facilitate the development of an integrative therapeutic strategy for chronic muscle pain.

Although the involvement of NET-mediated processes in numerous painful diseases, including gout and rheumatoid arthritis, has been reported [21, 22], no reports have described the relationship between NETs and muscle pain. Therefore, using a muscle pain model with muscle overuse, we examined whether neutrophils play a key role in developing muscle pain via NET production triggered by increased uric acid levels.

Methods

Experimental animals

Male BALB/c mice (5–7 weeks old) were used in this study (CLEA Japan, Tokyo, Japan). The experimental design, care, and use of the mice were performed according to the guidelines for animal experiments at Tohoku University. Ethical approval for this study was obtained from the Animal Research

Committee of Tohoku University (approval number: 2019 MdA-070). The mice were kept in standard cages maintained in an air-conditioned room at 23 °C ± 1 °C with a 12-h light–dark cycle with ad libitum access to standard food pellets and tap water, in accordance with the National Standards Relating to the Care and Management of Laboratory Animals and Relief of Pain (Notification No. 88 of the Ministry of the Environment, Japan, April 28, 2006). General anesthesia was induced in each mouse by the intraperitoneal injection of medetomidine (0.3 mg/kg; ZENOAQ, Fukushima, Japan), midazolam (4.0 mg/kg; SANDZ, Tokyo, Japan), and butorphanol (5.0 mg/kg; Meiji Seika Pharma Co, Tokyo, Japan). Mice were sacrificed by cervical dislocation under inhalation anesthesia with isoflurane (MSD Animal Health, Kenilworth, NJ, USA).

Repeated electrical stimulation of the triceps surae muscles

Electrical pulse stimulation (EPS) was repeatedly applied to induce excessive muscle contraction of the TSMs, as previously described [10, 11, 17]. Two stainless electrodes (single-stranded stainless steel wire, A-M system, Sequim, WA, USA) were transcutaneously inserted into the proximal and distal ends of the TSMs on the dorsal surface of the hindlimbs under anesthesia. EPS using a STG4004 multichannel system (MCS GmbH, Reutlingen, Germany) was performed on the muscle at 10 Hz with a 10-V amplitude and a 100-μs pulse width for 30 min everyday (day 0 through day 6). The bilateral hindlimbs were immobilized with full ankle dorsiflexion using a scotch tape to stabilize the static muscle tension during EPS. Electrodes were also applied to the contralateral hindlimbs without EPS. Within 24 h after the last EPS, the TSMs were collected, immediately frozen in liquid nitrogen, and stored at -80 °C until assayed.

Assessment of mechanical nociceptive thresholds

The mechanical nociceptive threshold (MNT) was defined as the amount of pressure required to evoke pain-related reactions such as vocalization, struggling, and hindlimb withdrawal. The MNT was evaluated using the Randall–Selitto test (MK-201D Pressure Analgesy-Meter, Muromachi Kikai Co., Tokyo, Japan) [24]. The test was performed with a cone-shaped, 2.6-mm-diameter tip attached to a scale with a display. Pressure, gradually increasing at regular intervals (10 mmHg/s), was applied to the lateral side of the TSMs. We set the cut-off value to 300 mmHg, as previously described [11]. Since circadian rhythm affects pain sensitivity, all MNT measurements were performed in the morning. To avoid bias, the MNT assessments were analyzed by an investigator who was blinded to the experimental conditions.

Local effect of monosodium urate stimulation

To confirm the local effects of MSU on NET induction, recrystallized MSU (No. 133–13432; Wako Pure Chemicals Industries, Osaka, Japan) dissolved in saline was administered to the right TSMs (MSU

group), as previously described [25, 26]. Saline was administered to the contralateral TSMs (control group). The solution (100 µL) of recrystallized MSU (200 µg) was injected under the fascia of the lateral head of the TSMs using a 27-gauge needle. MNTs were assessed on days 0, 1, 2, and 4 post-injection. The TSMs were obtained, frozen in liquid nitrogen, and stored at -80 °C until assayed.

Pharmacological experiments related to neutrophil extracellular trap formation

We administered deoxyribonuclease (DNase) I (Wako Pure Chemical Industries, Ltd., Osaka, Japan; 10 mg per kg body weight [BW] per day) through intravenous injection via the tail vein [27] or febuxostat (F0847, Tokyo Chemical Industry Co., Ltd., Tokyo, Japan; 5 mg per kg BW per day) through intraperitoneal injection [28]. The control mice were injected with the same volume of the control vehicle (saline) 15 min prior to the experiment.

To deplete neutrophils, anti-granulocyte-differentiation antigen 1 (Gr-1; a major neutrophil marker) antibody (RB6-8C5, rat IgG2b) purified from the culture supernatants of a hybridoma (provided by Dr. R. Coffman) was intravenously administered into the mice (Gr-1 group) once every 3 days at a dose of 5 mg/kg BW [29, 30], because the injection effectively causes neutropenia for at least a few days [31, 32]. The control mice were also injected with an equivalent amount of normal rat IgG (Jackson Laboratories, Bar Harbor, ME, US) (IgG group).

-

Measurement of tissue uric acid levels

The frozen muscles (30 mg) were homogenized using Micro Smash MS-100R (Takara Tommy, Tokyo, Japan) in 300 µL of lysis buffer (30 mM Tris, 100 mM sodium chloride, 1 mM ethylenediaminetetraacetic acid, 1% Triton X-100, 2.5 mM sodium fluoride, 2 mM sodium polyphosphate, 1 mM sodium orthovanadate, 1 mM phenylmethylsulphonyl fluoride, 10 µg/mL aprotinin, 1 µg/mL pepstatin, and 5 µg/mL leupeptin) and then the lysate was centrifuged at 12,000 × g for 15 min at 4 °C. The supernatants were collected for uric acid assay and western blotting. The tissue levels of uric acid were measured using an assay kit (700320, Cayman Chemical Company, Ann Arbor, USA) following the manufacturer's instructions.

Quantitative reverse transcription polymerase chain reaction

Total RNA was extracted from the TSM tissues using TRIzol (Molecular Research Centre Inc., Cincinnati, OH, USA) and Micro Smash MS-100R (Takara Tommy, Tokyo, Japan). cDNA was prepared using a Transcriptor First Strand cDNA Synthesis Kit (Roche, Basel, Switzerland). The primer sequences used were as follows: IL-1b: F5'-TGG TGG GGG TTC TCT GTG GTT-3' and R5'-TTG AGG CGG CTT TCT TTG

TCC-3′ and EF1a1 (internal control primer): F5′-TCG CTT TGC TGT TCG TGA C-3′ and R5′-TGG GGT GGC AGG TGT TAG-3′. The relative expression levels of each mRNA were calculated as a function of EF1a1 expression, as previously described [11, 17].

Immunohistochemistry

The dissected TSM tissues were snap-frozen in liquid nitrogen and embedded in a Tissue-Tek optimum cutting temperature compound (Sakura Finetek, Tokyo, Japan). The cryosections were transversely cut into 5-μm-thick sections using a cryostat (CM1850; Leica, Nussloch, Germany) and mounted on coated glass slides (MAS-coated; Matsunami Glass, Osaka, Japan). The sections were fixed with acetone. After washing in phosphate-buffered saline (PBS), endogenous immunoglobulins were blocked by incubation with a blocking buffer (5% bovine serum albumin [BSA] in Tris-buffered saline with 0.1% Tween-20) and 10% normal goat serum (Nichirei Biosciences Inc., Tokyo, Japan) for 30 min. The slides were incubated with a polyclonal rabbit anti-citH3 antibody (ab5103; 10 ng/mL; Abcam, Waltham, USA) and anti-Gr-1 antibody (RB6-8C5, rat IgG2b; 10 ng/mL; BioLegend, San Diego, CA, USA) in a blocking buffer for 2 h at room temperature (RT). PBS was used to rinse the slides. Subsequently, the slides were incubated for 1 h in PBS with an Alexa Fluor 488-conjugated goat anti-rabbit IgG (A-11034, Life Technologies, Carlsbad, CA, USA; dilution, 1:750) for anti-citH3 and an Alexa Fluor 555-conjugated goat anti-rat IgG (A- 21434, Life Technologies; dilution, 1:750) for Gr-1 at RT. The slides were once again rinsed with PBS. Finally, the slides were incubated with 4,6-diamidino-2-phenylindole (Sigma–Aldrich; dilution, 1:500) for 10 min at RT for nuclear staining. Images were captured using a fluorescence microscope (Olympus FV1000; Olympus, Tokyo, Japan) equipped with an oil-immersion objective lens (UApo/340 40×/NA 1.35). The images were analyzed using Fiji/ImageJ software (NIH, Bethesda, MD, USA). At least three images from each slide were captured at 200X magnification. To avoid bias, a few animals were used for immunohistochemistry (IHC), and two slides/animals were analyzed. After confirming the reproducibility, representative images were obtained.

-

Immunoblotting

The tissue lysates extracted from the TSM tissues were adjusted to 4.0 mg/mL with a lysis buffer using a BCA Protein Assay Kit (Thermo Fisher Scientific, Waltham, MA, USA). In brief, 30 μL of samples were loaded for 5%–12% sodium dodecyl sulphate–polyacrylamide gel electrophoresis and transferred to Immobilon-P polyvinylidene difluoride membranes (Merck, Kenilworth, NJ, USA) for immunoblotting [33]. The protein-transferred membranes were blocked with 5% BSA in Tris-buffered saline with 0.1% Tween-20 and then incubated at 4 °C overnight with anti-citH3 (ab5103; 2 μg/mL), anti-histone H3 (ab1791; 1 μg/mL; Abcam, Waltham, USA), anti-lymphocyte antigen 6 superfamily of the glycosylphosphatidylinositol-linked protein (Ly6G; BioLegend 127602; 2 μg/mL; Biolegend, San Diego, CA, USA), and anti-glyceraldehyde 3-phosphate dehydrogenase (GAPDH) (#2118; 1:1000 dilution; Cell

Signaling, Beverly, MA, USA). The membranes were washed with Tris-buffered saline containing 0.1% Tween-20, followed by incubation at RT for 1 h with horseradish peroxidase-conjugated secondary antibodies (1:10,000 dilutions of #ab6734; Abcam, Cambridge, UK; and 1:5,000 dilutions of #32460; Thermo Fisher Scientific, Waltham, MA, USA). Next, a signal was produced using a chemiluminescence reagent, obtained from SuperSignal West Femto Maximum Sensitivity Substrate (Thermo Fisher Scientific, Waltham, MA, USA), and the saturated band intensity was detected using the Image Quant TL system (GE Healthcare, Chalfont St Giles, UK).

-

Multiphoton microscopy imaging using in vivo staining of NET-like structures

To detect NETs through in vivo staining, two types of fluorescent reagents, anti-Gr-1 antibody conjugated to Qdot655 (QD-Gr-1Ab, 3.0 μg per mouse) to detect neutrophils and SYTOX Green (Thermo Fisher Scientific, 1 μL of 5 mM solution per mouse) to detect extracellular DNA, were used [33-35], and anti-Gr-1 antibodies were prepared by conjugation to Qdot 655 using the SAIVI rapid antibody labeling kit from Invitrogen. The conjugate was purified using a size-exclusion column, and its concentration was determined by measuring the absorbance at 679 nm and calculated using the extinction coefficient (180,000 M−1 cm−1). After 24 h from EPS on day 7, QD-Gr-1Ab and SYTOX were injected via the tail vein at 20 min before animal sacrifice under anesthesia. Mice were fixed by transcardiac perfusion with 4% paraformaldehyde/PBS, and the TSM tissues were subjected to multiphoton microscopy (MPM) imaging. An upright A1R-MP multiphoton microscope (Nikon) equipped with a Ti-sapphire laser (Mai-Tai Deep See, Spectra-Physics), GaAsP non-descanned detectors, and a water-immersion objective lens (CFP75 Apo LWD 25x/NA1.1) was used for image recording with an excitation laser consistently set at 920 nm, with an area size of 510 μm × 510 μm and a resolution of 600 dpi. The wavelengths for detection using emission filter cubes were 492/SP nm for second-harmonic generation signals (blue channel), 525 ± 50 nm for SYTOX (green channel), and 629 ± 56 nm for QD-Gr-1Ab (far-red channel). By distinguishing between the muscle and myofascial area based on the second-harmonic generation signals indicating muscle and collagenous fibers [36], we obtained the fluorescence colocalization of QD-Gr-1Ab and SYTOX to quantitatively measure the accumulation of NET-like structures in each area using ImageJ software [37]. Further, representative 3D image stacks focusing on neutrophil recruitment releasing extracellular DNA were reconstructed from the sequential images in TSM structure.

Statistical analysis

Statistical analyses were performed using SPSS Statistics 27 (IBM, Armonk, NY, USA). Analysis of the MNT time-course data was performed using two-way analysis of variance (ANOVA), and repeated measurements were compared using Tukey’s post-hoc multiple-comparison test. To compare data from more than three groups from single and multiple days, one-way and two-way ANOVA with Tukey’s post-hoc multiple comparison test were used for the analysis, respectively. Western blotting and IL-1β data

between the two groups were analyzed using the Wilcoxon signed-rank test. Other data between the two groups were analyzed using paired t-tests. All data are expressed as the mean ± standard error of the mean. Statistical significance was set at $P < 0.05$.

Results

MSU stimulation induces NETs and muscle pain in the TSMs

To investigate whether MSU crystals induced NETs in skeletal muscle tissues, as shown in previous studies, we first performed the intramuscular injection of MSU by following a method reported in our previous study (Fig. 1) [11]. Compared to those of the control group, the MNTs of the MSU group significantly decreased after the intramuscular injection of MSU (Fig. 1a). In terms of IHC observations, control TSMs with saline injection did not show any changes, whereas the increased immunoreactivity of citH3 and Gr-1 was located around the outer edge of MSU (Fig. 1b). Western blotting using the TSM tissues stimulated with MSU on day 2 showed significant increases in citH3 (Fig. 1c) and Ly6G (Fig. 1d). Additionally, IL-1β expression in the TSMs injected with MSU significantly increased on day 2 (Fig. 1e).

-

Excessive muscle contraction caused by repeated EPS induced mechanical hyperalgesia with elevated NET production in the skeletal muscle tissues

We next confirmed whether excessive muscle contraction by EPSs induced NET formation associated with an increase in tissue uric acid levels (Fig. 2). As previously shown in our studies [11, 17], the MNTs of the stimulated TSMs significantly decreased due to repeated stimulation, compared to those of the contralateral muscle, and were significantly decreased, with the minimum MNT noted on day 7 (Fig. 2a). Reduced MNTs in the stimulated TSMs increased again after 7 consecutive days of electrical stimulation, and MNTs between the control (non-stimulated) and MSU (stimulated) groups were not significant on day 11 (Fig. 2a). The tissue samples on day 7 were mainly used in our analyses based on the above results. Among the TSM samples on day 7, tissue uric acid levels in the stimulated TSMs were significantly higher than those in the contralateral TSMs (Fig. 2b).

IHC analysis indicated distinct distribution patterns of citH3 immunoreactivities, which colocalized with Ly6G immunoreactivities in the stimulated TSMs, but not in the non-stimulated TSMs (Fig. 2c). Hematoxylin and eosin staining showed typical skeletal muscle tissue histology in both groups (data not shown). Further confirming these observations, western blotting indicated that the relative density of citH3 (Fig. 2d) and Ly6G (Fig. 2e) normalized to the loading control (total H3 and GAPDH, respectively) were significantly increased in the stimulated TSMs on day 7 compared with those in the non-stimulated TSMs. The time-series experiment of citH3 protein in comparison with ipsilateral to contralateral TSM tissues during and after EPS is shown in Fig. 2f. The protein amount ratio of citH3 showed the highest value on day 7 with repeated EPS, whereas it recovered to the level on day 0 after stopping the

stimulation. IL-1β mRNA expression was significantly increased in the stimulated TSMs than in the non-stimulated TSMs (Fig. 2g).

DNase treatment ameliorated muscle hyperalgesia and NET induction owing to repeated EPS

To confirm the pathological significance of NETs in muscle hyperalgesia, we administered DNase I to degrade extracellular DNA, including NETs, and demonstrated its impact on muscle hyperalgesia (Fig. 3). Intravenous administration of DNase I significantly increased the MNT values (Fig. 3a) and decreased tissue uric acid levels (Fig. 3b) in the stimulated TSMs. Consistent with these observations, IHC (Fig. 3c) and western blotting analyses (Fig. 3d and e) indicated that DNase I administration decreased the citH3 expression, but not the protein concentration of Gr-1. Additionally, IL-1β mRNA expression in the stimulated TSMs decreased following DNase I administration (Fig. 3f). Importantly, DNase administration reduced not only citH3, but also tissue uric acid levels despite the same intensity and duration of the repeated EPS application.

Neutrophil depletion ameliorated muscle hyperalgesia and NET induction owing to repeated EPS

Given the absolute necessity of neutrophil recruitment for NET induction, we next examined the effects of an experimental neutrophil depletion by prior treatment with anti-Gr-1 antibody on muscle hyperalgesia (Fig. 4). Neutrophil depletion resulted in a significant increase of the MNT in the stimulated hindlimbs (Fig. 4a) and reduced tissue uric acid levels (Fig. 4b) in the TSMs with repeated EPS. Similar to the IHC images showing weaker immunoreactivity of citH3 and Gr-1 in the neutrophil-depleted group than in the control group (Fig. 4c), neutrophil depletion significantly decreased the relative ratio of citH3 (Fig. 4d) and IL-1β mRNA expression (Fig. 4e) in the stimulated TSMs compared with the control mice injected with the same amount of normal rat IgG. Notably, the tissue uric acid level in the stimulated TSMs was decreased with experimental neutrophil depletion.

Febuxostat treatment relieved muscle hyperalgesia due to repeated EPS

Since our recent study reported that the decrease in tissue uric acid levels resulted in the improvement of muscle hyperalgesia [11], we investigated whether the administration of febuxostat, a xanthine oxidase inhibitor, influenced NET induction due to repeated EPS (Fig. 5). As reported in our previous study [11], febuxostat treatment increased the MNTs (Fig. 5a), and reduced tissue uric acid levels (Fig. 5b) and IL-1β mRNA expression (Fig. 5f) in the stimulated TSMs. Consistent with these observations, IHC (Fig. 5c) and western blotting analyses indicated that febuxostat administration reduced citH3 expression (Fig. 5d), but not neutrophil recruitment (Fig. 5c and e) in the stimulated TSMs. These results indicate that high

tissue uric acid levels would play a central role in NET induction in skeletal muscle tissues with hyperalgesia.

MPM imaging with in vivo staining for NET-like structures

To confirm that repeated EPS induced neutrophil recruitment with extracellular DNA release in TSM tissues, MPM imaging was performed using an in vivo immunostaining method [35]. As shown in Fig. 6 and Supplemental movie, repeated EPS significantly increased the fluorescence of neutrophils and extracellular DNA in TSM tissues, as visualized by QD655 and SYTOX, respectively. In particular, the myofascial region showed significantly more fluorescence colocalizations than the TSM myofibers.

Discussion

The present study clarified the potential pathogenesis of NETs in muscle hyperalgesia (exhibiting elicited nocifensive behaviors) due to a locally higher tissue level of uric acids caused by excessive muscle contraction (Fig. 2) as well as noted the observations in the TSMs with MSU injection (Fig. 1). Our findings showed a potentially “vicious cycle” model of muscle hyperalgesia due to a higher tissue uric acid level, which develops in a reciprocal manner between neutrophil recruitment and NET induction (Fig. 7).

NETs play an essential function in immobilizing and killing pathogens, including bacteria, whilst limiting inflammation, whereas inappropriate NET release has harmful late effects on tissues due to the release of cytotoxic and proinflammatory mediators with NET degradation [22, 23]. Delayed-onset muscle soreness, a typical muscle pain experienced after excessive exercise, persists for a few days [7]. Based on the increased serum NET levels after acute severe exercise [38], the characteristics of NETs would not only play a crucial role in prolonging and strengthening local inflammation and pain, as observed in our results, but also in general muscle physiology. Additionally, recent studies have focused on the implications of NETs in numerous autoinflammatory diseases, including systemic lupus erythematosus, psoriasis, and gout [21, 22, 39]. Interestingly, our results also demonstrated that febuxostat administration, as well as the experimental neutrophil depletion and DNase administration, improved the local NET accumulation associated with muscle hyperalgesia (Fig. 3). Febuxostat was reported to reduce not only tissue uric acid content, but also neutrophil recruitment in damaged tissues [40]. Thus, local NET accumulation in skeletal muscles damaged by repeated excessive exercise would enhance inflammation and pain with a sustainable supply of proinflammatory stimuli consisting of inflammatory mediators, such as IL-1β and DAMPs, including uric acid.

MSU crystallization due to hyperuricemia is a typical causative stimulus of acute and painful inflammatory responses in gout attacks [20, 21]. Since our previous work showed that a higher uric acid level in skeletal muscle tissues was a potential trigger for muscle hyperalgesia [11], we here indicated the involvement of NETs as a crucial mediator in developing muscle hyperalgesia caused by a higher uric

acid content in skeletal muscle tissues. However, no MSU crystals were found in the skeletal muscle tissues with excessive contraction. In terms of MSU crystallization, Martillo et al. indicated that 405 μmol/L is the solubility limit of uric acid in the serum [41]. Our results showed that the average local uric acid concentration (approximately 500 μmol/L) in the stimulated muscles was higher than the abovementioned value. Because Braga et al. indicated that high concentrations of soluble uric acid directly activate innate immunity [16], a higher tissue uric acid level possibly contributes to the modulation of a microenvironment with a higher risk of NET induction as neutrophil recruitment.

In terms of a vicious cycle of a higher tissue uric acid level leading to NET accumulation and consequent development of muscle hyperalgesia (Fig. 7), both neutrophil depletion (Fig. 4) and DNase treatment (Fig. 3) essentially resulted not only in the improvement of muscle hyperalgesia, but also in the reduction of the tissue uric acid levels in the damaged skeletal muscles, as well as the febuxostat treatment (Fig. 5). Based on the activation of the inflammasome pathway in macrophages by a higher uric acid level [11, 16, 26], the neutrophil–macrophage interactions, as the main innate immune response, definitively contribute to the deterioration of muscle hyperalgesia. Although future studies with appropriate designs are warranted to clarify the above aspects, these findings suggest that extracellular DNA consisting of NETs with neutrophil recruitment is potentially the main source inducing a higher uric acid level in skeletal muscle tissues via purine metabolism and plays a role in exacerbating muscle hyperalgesia.

Furthermore, MPM imaging of NET-like structures showed that extracellular DNA fragments were mostly colocalized with neutrophils, but not in the skeletal muscle fibers. Shinoda et al. also reported no histological changes in the stimulated skeletal muscle tissues under the same experimental conditions [10]. Thus, a higher tissue uric acid content with skeletal muscle overloading may predominantly depend on neutrophil recruitment followed by NETosis. Furthermore, neutrophils releasing extracellular DNA were predominantly recruited more in myofascial tissues than in muscle fibers (Fig. 6). This is consistent with the multiple lines of evidence regarding the pathomechanisms underlying the development of MPS with the characteristic irritable response in myofascial tissues [15]. Future studies are warranted to clarify the mechanisms that dominantly recruit neutrophils in myofascial tissues, thus providing new insights regarding MPS therapy and management.

Conclusions

Our findings of NET dynamics clarified the underlying mechanism of muscle hyperalgesia associated with recruited neutrophils forming NETs, which potentially cause a higher uric acid content in skeletal muscle tissues. Thus, the regulation of local uric acid metabolism while focusing on NET induction would be a potential therapeutic target to relieve muscle pain.

Abbreviations

ANOVA, analysis of variance; ATP, adenosine triphosphate; DAMP, damage-associated molecular pattern; DAPI, 4,6-diamidino, 2-phenylindole; DNase, deoxyribonuclease; EPS, electrical pulse stimulation; IHC,

immunohistochemistry; IL, interleukin; Ly6G, lymphocyte antigen 6 superfamily of the glycosylphosphatidylinositol-linked protein; GAPDH, glyceraldehyde 3-phosphate dehydrogenase; Gr-1, granulocyte receptor-1 antigen; citH3, citrullinated histone H3; MPM, multiphoton microscopy; MPS, myofascial pain syndrome; MSU, monosodium urate; MNT, mechanical withdrawal threshold; NETs, neutrophil extracellular traps; PBS, phosphate-buffered saline; QD, Quantum dot; RT, room temperature; TSM, triceps surae muscle.

Declarations

Ethics approval and consent to participate

The experimental design, care, and use of the mice were performed according to the guidelines for animal experiments at Tohoku University. Ethical approval for this study was obtained from the Animal Research Committee of Tohoku University (approval number: 2019 MdA-070).

Consent for publication

Not applicable

Availability of data and materials

The data that support the findings of this study are available from the corresponding author, MT, upon reasonable request.

Competing interests

The authors declare that they have no competing interests.

Funding

This work was supported in part by grants from the Japan Society for the Promotion of Science (nos. 16K11580 and 19K10229 to MT).

Authors' contributions

Conceptualization: KS, MT, SY, MK, and YH; Data curation: KS, MT, and KO; Formal analysis: KS and MT; Funding acquisition: MT, SY, MK, and YH; Investigation: KS, SY, KO, WC, TT, RF, and YL; Methodology: KS, MT, WC, MK, and YL; Project administration: MT, SY, MK, YY, and YH; Resources: KS, MT, SY, KO, WC, TT, RF, and YL; Supervision: MK, TA, and YH; Validation: TT, RF, and YL; Writing – original draft: KS, MT, SY, and YH. All authors contributed to the data analysis and work presented in this paper.

Acknowledgments

The authors are grateful to Dr. Shigenori Sekiai, Dr. Chayanit Chaweewannakorn, and Ms. Natsumi Emoto at the Tohoku University Graduate School of Biomedical Engineering for their technical assistance and Dr.

Hiroyuki Tada at the Tohoku University Graduate School of Dentistry for the excellent advice on the study. We also thank other doctors at the Department of Orthopaedic Surgery, Tohoku University Graduate School of Medicine, for their excellent technical advice in this study.

References

1. Fayaz A, Croft P, Langford RM, Donaldson LJ, Jones GT: Prevalence of chronic pain in the UK: a systematic review and meta-analysis of population studies. BMJ Open 2016, 6:e010364. https://doi.org/10.1136/bmjopen-2015-010364.

2. Hanvold TN, Waersted M, Mengshoel AM, Bjertness E, Stigum H, Twisk J, et al: The effect of work-related sustained trapezius muscle activity on the development of neck and shoulder pain among young adults. Scand J Work Environ Health 2013, 39:390-400. https://doi.org/10.5271/sjweh.3357.

3. van Dieen JH, Selen LP, Cholewicki J: Trunk muscle activation in low-back pain patients, an analysis of the literature. J Electromyogr Kinesiol 2003, 13:333-351. https://doi.org/10.1016/s1050-6411(03)00041-5.

4. Borg-Stein J, Simons DG: Focused review: myofascial pain. Arch Phys Med Rehabil 2002, 83:S40-47, S48-49. https://doi.org/10.1053/apmr.2002.32155.

5. Punnett L, Wegman DH: Work-related musculoskeletal disorders: the epidemiologic evidence and the debate. J Electromyogr Kinesiol 2004, 14:13-23. https://doi.org/10.1016/j.jelekin.2003.09.015.

6. Mills SEE, Nicolson KP, Smith BH: Chronic pain: a review of its epidemiology and associated factors in population-based studies. Br J Anaesth 2019, 123:e273-e283. https://doi.org/10.1016/j.bja.2019.03.023.

7. Mense S: Muscle pain: mechanisms and clinical significance. Dtsch Arztebl Int 2008, 105:214-219. https://doi.org/10.3238/artzebl.2008.0214.

8. Mastaglia FL: The relationship between muscle pain and fatigue. Neuromuscul Disord 2012, 22 Suppl 3:S178-180. https://doi.org/10.1016/j.nmd.2012.10.003.

9. Dubin AE, Patapoutian A: Nociceptors: the sensors of the pain pathway. J Clin Invest 2010, 120:3760-3772. https://doi.org/10.1172/JCI42843.

10. Shinoda M, Ozaki N, Sugiura Y: Involvement of ATP and its receptors on nociception in rat model of masseter muscle pain. Pain 2008, 134:148-157. https://doi.org/10.1016/j.pain.2007.04.006.

11. Yoshida S, Hagiwara Y, Tsuchiya M, Shinoda M, Koide M, Hatakeyama H, et al: Involvement of inflammasome activation via elevation of uric acid level in nociception in a mouse model of muscle pain. Mol Pain 2019, 15:1744806919858797. https://doi.org/10.1177/1744806919858797.

12. Retamoso LT, Silveira MEJ, Lima FD, Busanello GL, Bresciani G, Ribeiro LR, et al: Increased xanthine oxidase-related ROS production and TRPV1 synthesis preceding DOMS post-eccentric exercise in rats. Life Sci 2016, 152:52-59. https://doi.org/10.1016/j.lfs.2016.03.029.

13. Green HJ, Fraser IG: Differential effects of exercise intensity on serum uric acid concentration. Med Sci Sports Exerc 1988, 20:55-59. https://doi.org/10.1249/00005768-198802000-00008.

14. Kono H, Chen CJ, Ontiveros F, Rock KL: Uric acid promotes an acute inflammatory response to sterile cell death in mice. J Clin Invest 2010, 120:1939-1949. https://doi.org/10.1172/JCI40124.

15. Chen R, Yin C, Fang J, Liu B: The NLRP3 inflammasome: an emerging therapeutic target for chronic pain. J Neuroinflammation 2021, 18:84. https://doi.org/10.1186/s12974-021-02131-0.

16. Braga TT, Forni MF, Correa-Costa M, Ramos RN, Barbuto JA, Branco P, et al: Soluble Uric Acid Activates the NLRP3 Inflammasome. Sci Rep 2017, 7:39884. https://doi.org/10.1038/srep39884.

17. Yoshida S, Hagiwara Y, Tsuchiya M, Shinoda M, Koide M, Hatakeyama H, et al: Involvement of neutrophils and interleukin-18 in nociception in a mouse model of muscle pain. Mol Pain 2018, 14:1744806918757286. https://doi.org/10.1177/1744806918757286.

18. Kastner DL, Aksentijevich I, Goldbach-Mansky R: Autoinflammatory disease reloaded: a clinical perspective. Cell 2010, 140:784-790. https://doi.org/10.1016/j.cell.2010.03.002.

19. Mutua V, Gershwin LJ: A Review of Neutrophil Extracellular Traps (NETs) in Disease: Potential Anti-NETs Therapeutics. Clin Rev Allergy Immunol 2020. https://doi.org/10.1007/s12016-020-08804-7.

20. Punzi L, Scanu A, Ramonda R, Oliviero F: Gout as autoinflammatory disease: new mechanisms for more appropriated treatment targets. Autoimmun Rev 2012, 12:66-71. https://doi.org/10.1016/j.autrev.2012.07.024.

21. Bodofsky S, Merriman TR, Thomas TJ, Schlesinger N: Advances in our understanding of gout as an auto-inflammatory disease. Semin Arthritis Rheum 2020, 50:1089-1100. https://doi.org/10.1016/j.semarthrit.2020.06.015.

22. Neubert E, Meyer D, Rocca F, Gunay G, Kwaczala-Tessmann A, Grandke J, et al: Chromatin swelling drives neutrophil extracellular trap release. Nat Commun 2018, 9:3767. https://doi.org/10.1038/s41467-018-06263-5.

23. Cicco S, Cicco G, Racanelli V, Vacca A: Neutrophil Extracellular Traps (NETs) and Damage-Associated Molecular Patterns (DAMPs): Two Potential Targets for COVID-19 Treatment. Mediators Inflamm 2020, 2020:7527953. https://doi.org/10.1155/2020/7527953.

24. Randall LO, Selitto JJ: A method for measurement of analgesic activity on inflamed tissue. Arch Int Pharmacodyn Ther 1957, 111:409-419.

25. Ju TJ, Dan JM, Cho YJ, Park SY: Inhibition of Inducible Nitric Oxide Synthase Attenuates Monosodium Urate-induced Inflammation in Mice. Korean J Physiol Pharmacol 2011, 15:363-369. https://doi.org/10.4196/kjpp.2011.15.6.363.

26. Chen CJ, Shi Y, Hearn A, Fitzgerald K, Golenbock D, Reed G, et al: MyD88-dependent IL-1 receptor signaling is essential for gouty inflammation stimulated by monosodium urate crystals. J Clin Invest 2006, 116:2262-2271. https://doi.org/10.1172/JCI28075.

27. Cagliani J, Yang WL, Brenner M, Wang P: Deoxyribonuclease Reduces Tissue Injury and Improves Survival After Hemorrhagic Shock. J Surg Res 2020, 249:104-113. https://doi.org/10.1016/j.jss.2019.11.036.

28. Wang S, Li Y, Song X, Wang X, Zhao C, Chen A, et al: Febuxostat pretreatment attenuates myocardial ischemia/reperfusion injury via mitochondrial apoptosis. J Transl Med 2015, 13:209. https://doi.org/10.1186/s12967-015-0578-x.

29. Chen L, Watanabe T, Watanabe H, Sendo F: Neutrophil depletion exacerbates experimental Chagas' disease in BALB/c, but protects C57BL/6 mice through modulating the Th1/Th2 dichotomy in different directions. Eur J Immunol 2001, 31:265-275. https://doi.org/10.1002/1521-4141(200101)31:1<265::AID-IMMU265>3.0.CO;2-L.

30. Hirano Y, Aziz M, Yang WL, Wang Z, Zhou M, Ochani M, et al: Neutralization of osteopontin attenuates neutrophil migration in sepsis-induced acute lung injury. Crit Care 2015, 19:53. https://doi.org/10.1186/s13054-015-0782-3.

31. Conlan JW, North RJ: Neutrophils are essential for early anti-Listeria defense in the liver, but not in the spleen or peritoneal cavity, as revealed by a granulocyte-depleting monoclonal antibody. J Exp Med 1994, 179:259-268. https://doi.org/10.1084/jem.179.1.259.

32. Rakhmilevich AL: Neutrophils are essential for resolution of primary and secondary infection with Listeria monocytogenes. J Leukoc Biol 1995, 57:827-831. https://doi.org/10.1002/jlb.57.6.827.

33. Chaweewannakorn C, Nyasha MR, Chen W, Sekiai S, Tsuchiya M, Hagiwara Y, et al: Exercise-evoked intramuscular neutrophil-endothelial interactions support muscle performance and GLUT4 translocation: a mouse gnawing model study. J Physiol 2020, 598:101-122. https://doi.org/10.1113/JP278564.

34. Masuda S, Shimizu S, Matsuo J, Nishibata Y, Kusunoki Y, Hattanda F, et al: Measurement of NET formation in vitro and in vivo by flow cytometry. Cytometry A 2017, 91:822-829. https://doi.org/10.1002/cyto.a.23169.

35. Sumagin R, Prizant H, Lomakina E, Waugh RE, Sarelius IH: LFA-1 and Mac-1 define characteristically different intralumenal crawling and emigration patterns for monocytes and neutrophils in situ. J Immunol 2010, 185:7057-7066. https://doi.org/10.4049/jimmunol.1001638.

36. Chaweewannakorn C, Harada T, Nyasha MR, Koide M, Shikama Y, Hagiwara Y, et al: Imaging of muscle activity-induced morphometric changes in fibril network of myofascia by two-photon microscopy. J Anat 2021, 238:515-526. https://doi.org/10.1111/joa.13339.

37. Tsuchiya M, Sekiai S, Hatakeyama H, Koide M, Chaweewannakorn C, Yaoita F, et al: Neutrophils Provide a Favorable IL-1-Mediated Immunometabolic Niche that Primes GLUT4 Translocation and Performance in Skeletal Muscles. Cell Rep 2018, 23:2354-2364. https://doi.org/10.1016/j.celrep.2018.04.067.

38. Syu GD, Chen HI, Jen CJ: Acute severe exercise facilitates neutrophil extracellular trap formation in sedentary but not active subjects. Med Sci Sports Exerc 2013, 45:238-244. https://doi.org/10.1249/MSS.0b013e31826df4a1.

39. Gray RD, Hardisty G, Regan KH, Smith M, Robb CT, Duffin R, et al: Delayed neutrophil apoptosis enhances NET formation in cystic fibrosis. Thorax 2018, 73:134-144. https://doi.org/10.1136/thoraxjnl-2017-210134.

40. Kataoka H, Yang K, Rock KL: The xanthine oxidase inhibitor Febuxostat reduces tissue uric acid content and inhibits injury-induced inflammation in the liver and lung. Eur J Pharmacol 2015, 746:174-179. https://doi.org/10.1016/j.ejphar.2014.11.013.

41. Martillo MA, Nazzal L, Crittenden DB: The crystallization of monosodium urate. Curr Rheumatol Rep 2014, 16:400. https://doi.org/10.1007/s11926-013-0400-9.

Figures

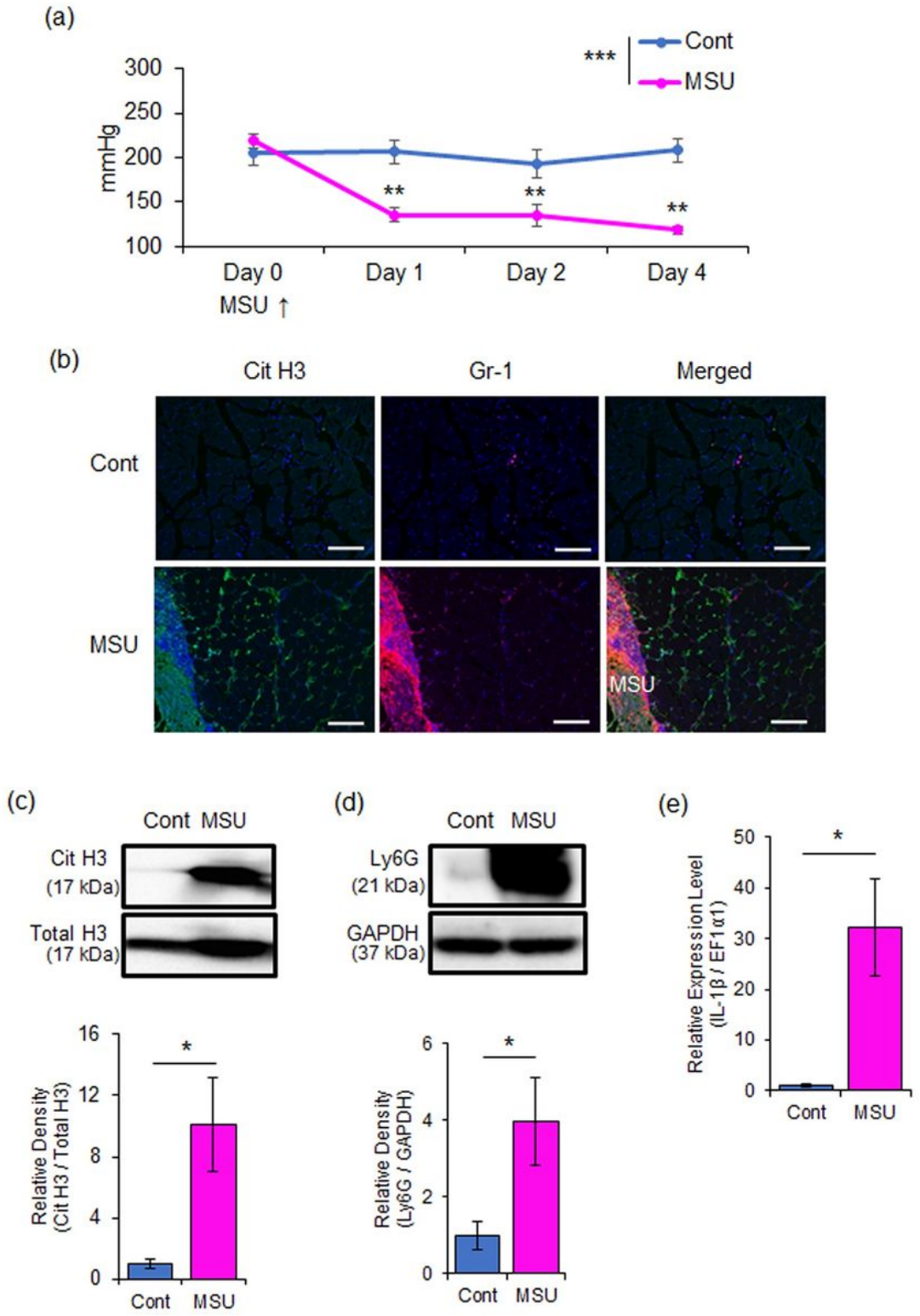

Figure 1

Induction of muscle hyperalgesia and NETs with intramuscular MSU injection. (a) Time-series experiment of MNT values in the MSU- or Saline-injected (contralateral) hindlimbs. (b) Representative IHC images of TSM tissue on day 2, indicating citH3 (green), Gr-1 (red), and DAPI (blue). Western blotting analysis of citH3 (c) and Ly6G (d) amounts in TSM tissues on day 2 after intramuscular injection of MSU or Saline. The relative density is normalized based on the loading control (total histone H3: total H3 and GAPDH,

respectively). Scale bar = 100 μm. (e) qRT-PCR analysis was performed to evaluate expression levels of IL-1β, using MSU- or saline-injected TSM tissues on day 2. All data are shown as mean ± SE (n = 6 - 10) and analysed using paired t-test or two-way ANOVA with Tukey's post-hoc multiple comparison test for time-series of MNT values. Statistical significance is indicated with * ($p < 0.05$), ** ($p < 0.01$) and *** ($p < 0.001$), respectively.

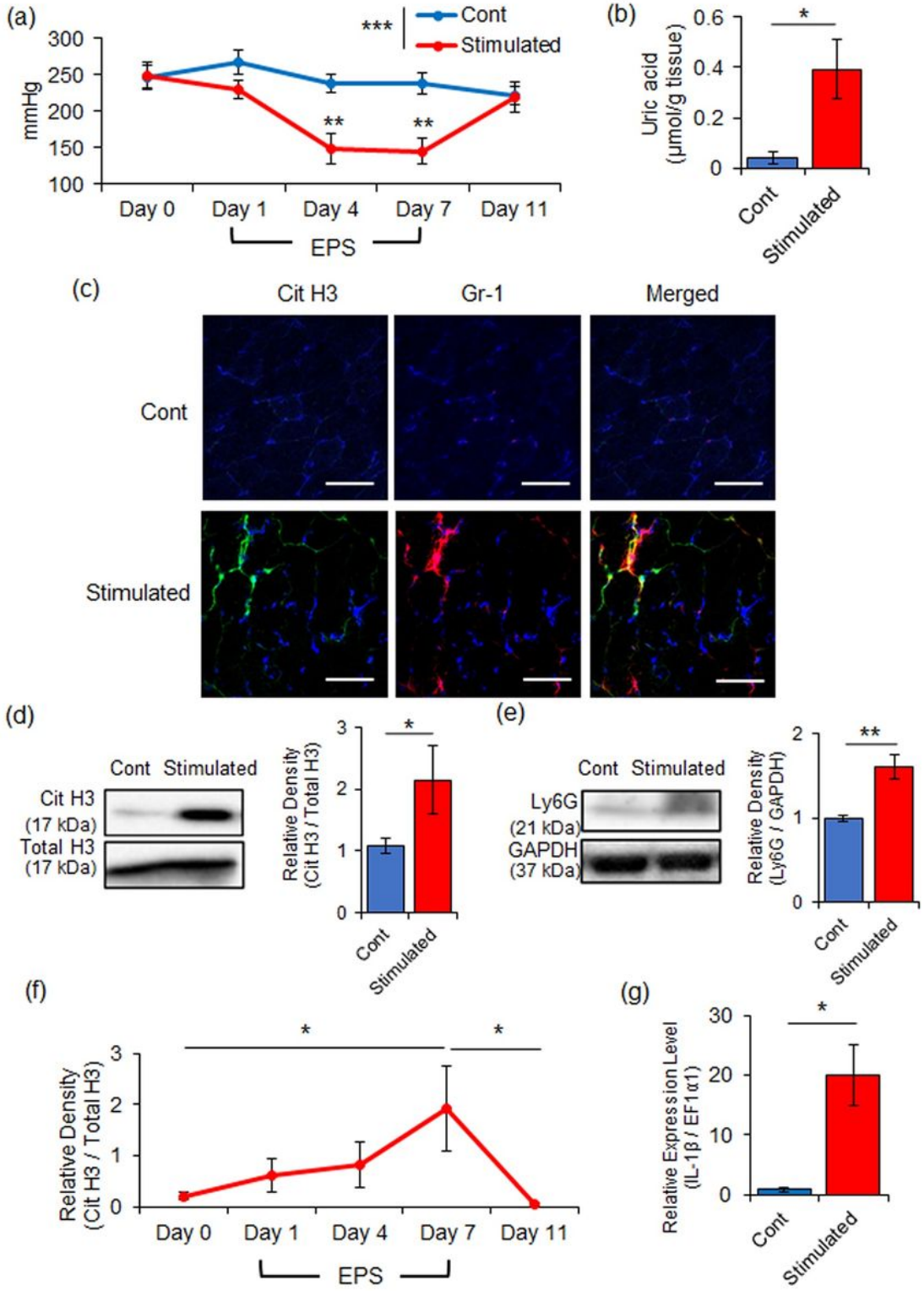

Figure 2

Effects of repeated electrical stimulation (EPS) to induce muscle hyperalgesia and NETs. (a) Time series experiment of MNT values in the stimulated and non-stimulated hindlimbs (contralateral side in the same mice). (b) The uric acid level in the stimulated and non-stimulated TSM tissues on day 7. (c) Representative IHC images of mouse TSM tissue with or without repeated EPS on day 7, indicating citH3 (green), Gr-1 (red), and DAPI (blue). Scale bar = 100 μm. (d) citH3 and (e) Ly6G amounts in TSM tissues with or without repeated EPS on day 7 by western blotting analysis. The relative density is normalized based on the loading control (total histone H3: total H3 and GAPDH, respectively). (f) Time series experiment of citH3 induction in stimulated TSM tissues. After normalization of citH3 using the total H3, a ratio of citH3 in ipsilateral side relative to contralateral side was calculated in each individual. (g) qRT-PCR analysis was performed to evaluate expression levels of IL-1β, using TSM tissues of control or stimulated mice on day 7. All data are shown as mean ± SE (n = 4 - 9) and analysed using paired t-test for comparing the mean of two different samples or two-way ANOVA followed by Tukey's post-hoc multiple comparison test for time-series experiment of MNT values and for comparing more than two groups. Statistical significance is indicated with * ($p < 0.05$), ** ($p < 0.01$) and *** ($p < 0.001$), respectively.

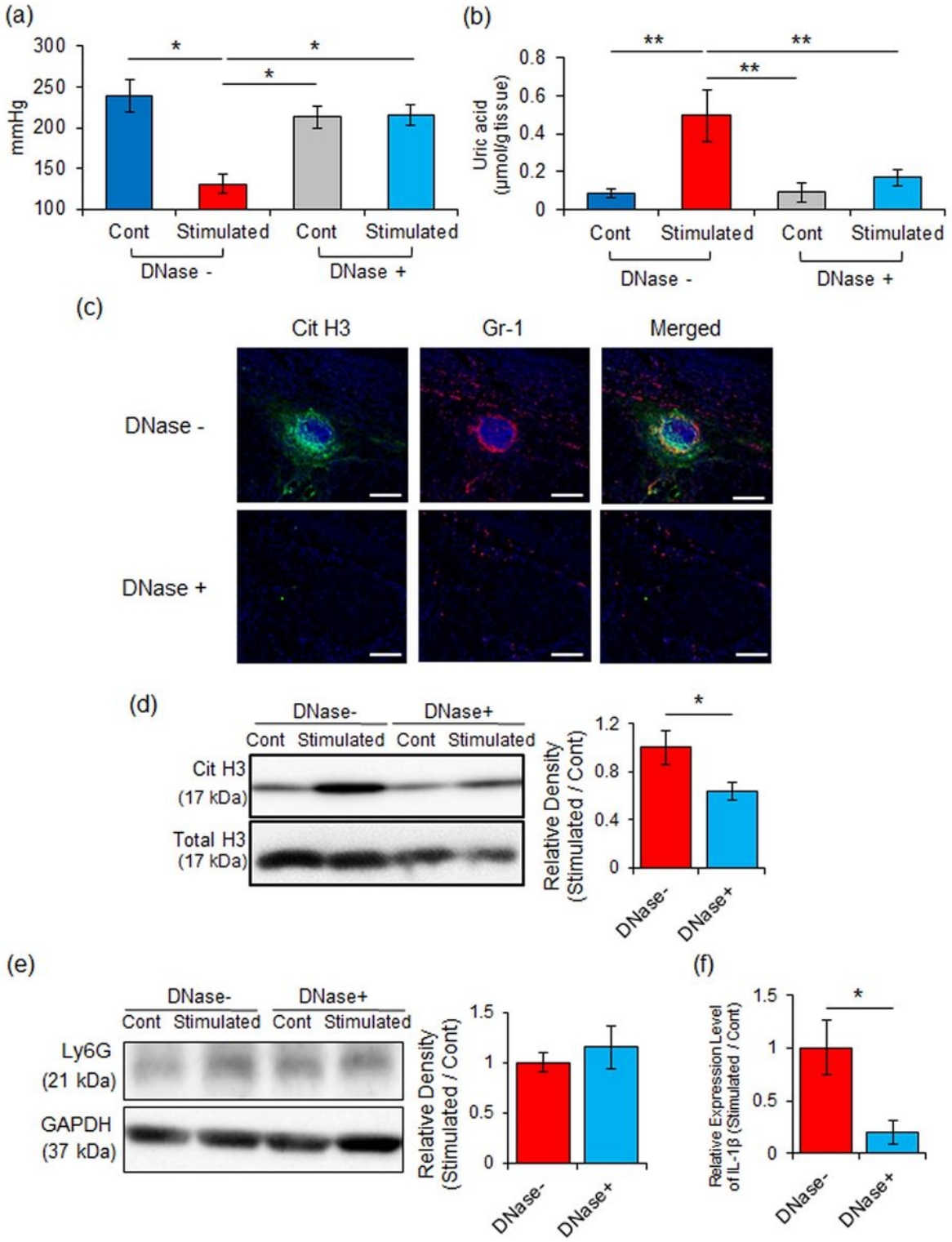

Figure 3

Effects of DNase treatment on NETs induction associated with muscle hyperalgesia. MNT values of hindlimbs (a) and the uric acid level (b) in TSM tissues in sham-stimulated control and stimulated mice injected intravenously with 10 mg/kg/day of DNase Ⅰ or a vehicle. (c) Representative IHC images of the stimulated TSM tissue with or without DNase Ⅰ administration on day 7, indicating citH3 (green), Gr-1 (red), and DAPI (blue). Scale bar = 100 μm. Western blotting analysis of citH3 (d) and Ly6G (e) amounts

in TSM tissues on day 7. The relative density is normalized based on the loading control (total H3 and GAPDH, respectively), and further calculated as a ratio in ipsilateral side relative to contralateral (unstimulated) side of the same individual. (f) qRT-PCR analysis was performed to evaluate expression levels of IL-1β in TSM tissues on day 7. All data are shown as mean ± SE (n = 4 - 9) and analysed using unpaired t-test for comparing the mean of two different samples or two-way ANOVA followed by post-hoc Tukey's test for a comparison of more than two groups. Statistical significance is indicated with * ($p < 0.05$), ** ($p < 0.01$) and *** ($p < 0.001$), respectively.

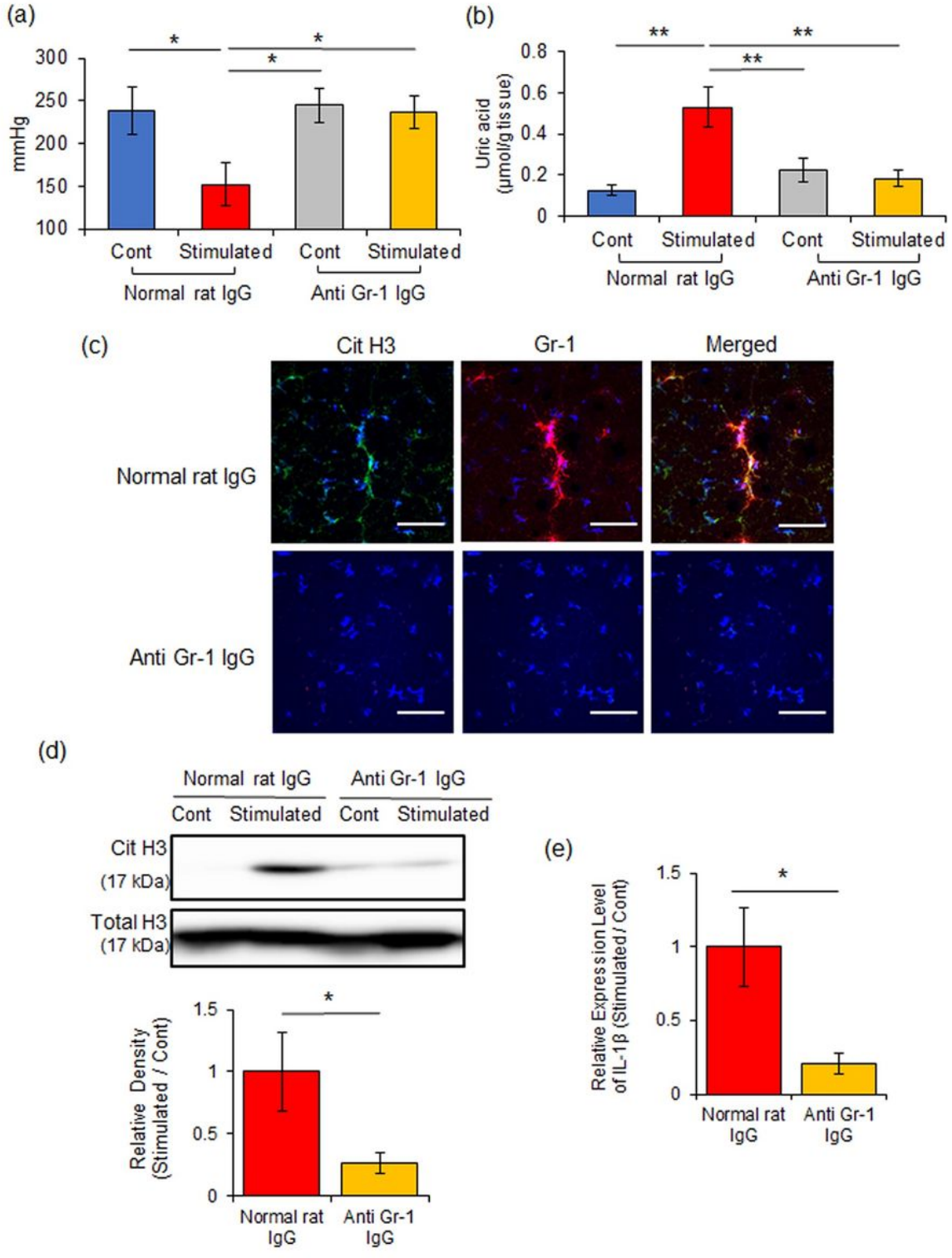

Figure 4

Effects of neutrophil depletion on NETs induction associated with muscle hyperalgesia. MNT values of hindlimbs (a) and the uric acid level (b) in TSM tissues in sham-stimulated control and stimulated mice injected intravenously with 5 mg/kg BW of anti-Gr-1 antibodies or control rat IgGs every 3 days. (c) Representative IHC images of the stimulated TSM tissue with or without neutrophil depletion on day 7, indicating citH3 (green), Gr-1 (red), and DAPI (blue). Scale bar = 100 μm. (d) Western blotting analysis of citH3 amounts in TSM tissues on day 7. The relative density is normalized based on the loading control (total H3), and further calculated as a ratio in ipsilateral side relative to contralateral (unstimulated) side of the same individual. (e) qRT-PCR analysis was performed to evaluate expression levels of IL-1β in TSM tissues on day 7. All data are shown as mean ± SE (n = 4 - 8) and analysed using unpaired t-test for comparing the mean of two different samples or two-way ANOVA followed by post-hoc Tukey's test for a comparison of more than two groups. Statistical significance is indicated with * ($p < 0.05$), ** ($p < 0.01$) and *** ($p < 0.001$), respectively.

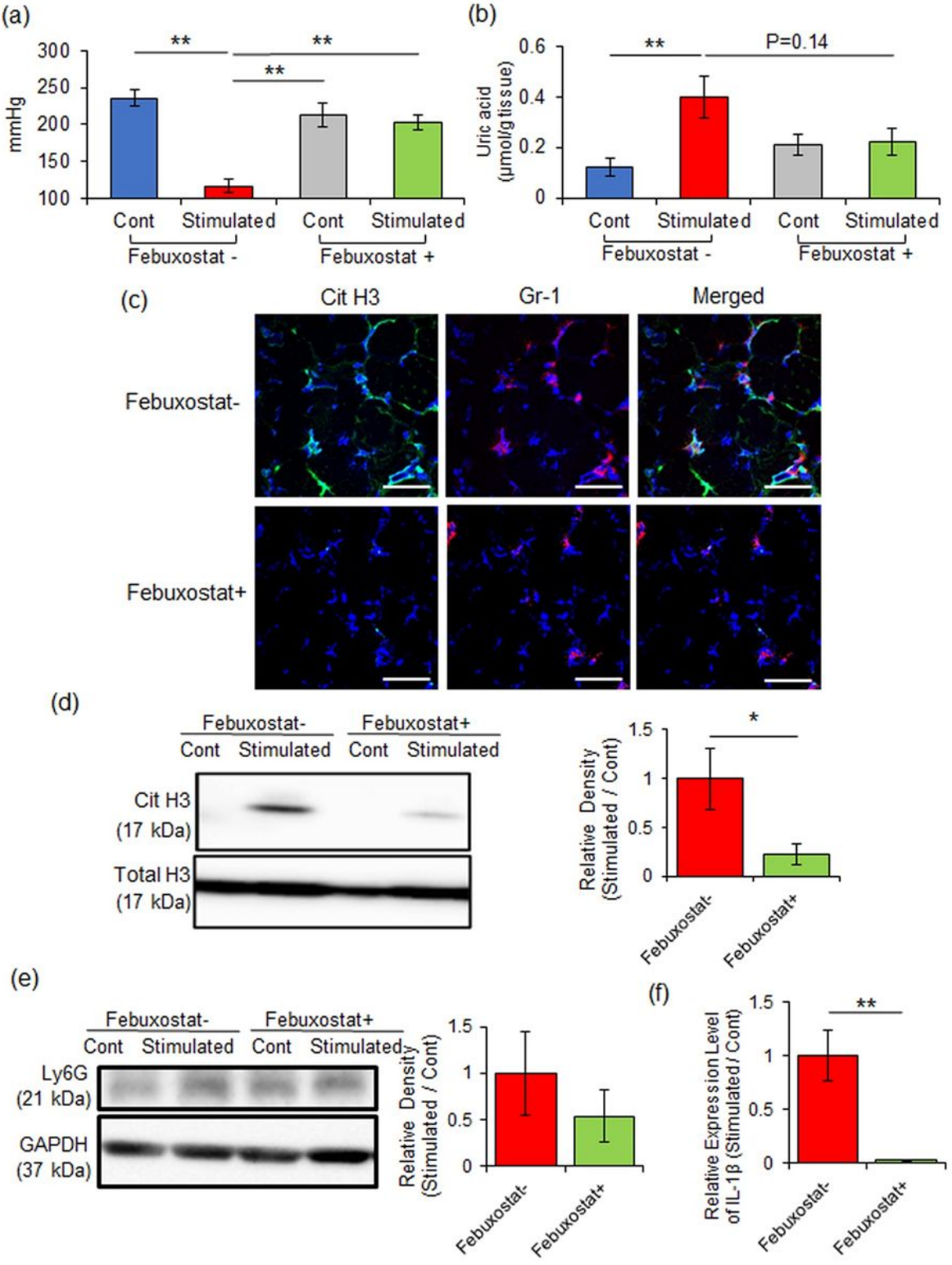

Figure 5

Effects of febuxostat treatment on NETs induction associated with muscle hyperalgesia. MNT values of hindlimbs (a) and the uric acid level (b) in TSM tissues in sham-stimulated control and stimulated mice injected intraperitoneally with 5 mg/kg BW/day of febuxostat or a vehicle. (c) Representative IHC images of the stimulated TSM tissue with or without febuxostat treatment on day 7, indicating citH3 (green), Gr-1 (red), and DAPI (blue). Scale bar = 100 μm. (d) Western blotting analysis of citH3 amounts in TSM tissues

with or without febuxostat treatment on day 7. The relative density is normalized based on the loading control (total H3), and further calculated as a ratio in ipsilateral side relative to contralateral (unstimulated) side of the same individual. (e) qRT-PCR analysis was performed to evaluate expression levels of IL-1β in TSM tissues on day 7. All data are shown as mean ± SE (n = 4 - 9) and analysed using unpaired t-test for comparing the mean of two different samples or two-way ANOVA followed by post-hoc Tukey's test for a comparison of more than two groups. Statistical significance is indicated with * ($p < 0.05$), ** ($p < 0.01$) and *** ($p < 0.001$), respectively.

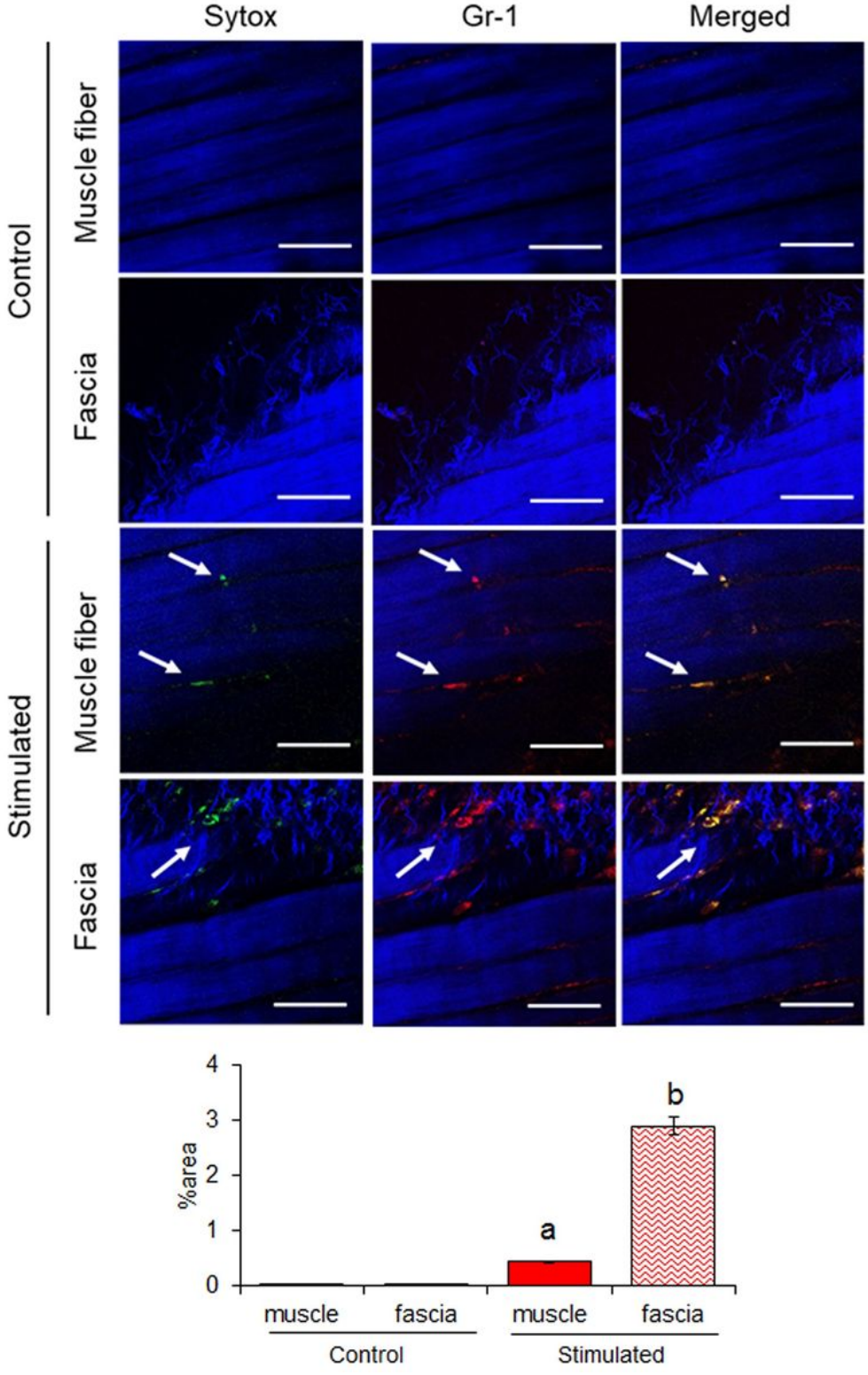

Figure 6

MPM imaging of neutrophil recruitment releasing extracellular DNA due to repeated electrical stimulation (EPS) as assessed by in vivo immunostaining. Representative images show fluorescence colocalization of neutrophils (indicated by white arrows) labelled with QD655-conjugated anti-Gr-1 antibody (red) and extracellular DNA labelled with SYTOX (green) in TSM tissues (muscle fibers and myofascia zone) of sham-control or stimulated mice on day 7. Muscle and collagenous fibers are visualized with second-harmonic generation (blue). The graph summarizing area quantification (%) of fluorescence colocalizations within myofascia or muscle fibers of TSM tissues is indicated. Data are shown as the mean ± SE (n = 3). The quantification results were analysed using one-way ANOVA with Tukey's post hoc test. Scale bar = 50 μm. Both a and b show significant difference to all other groups at $P < 0.05$, respectively.

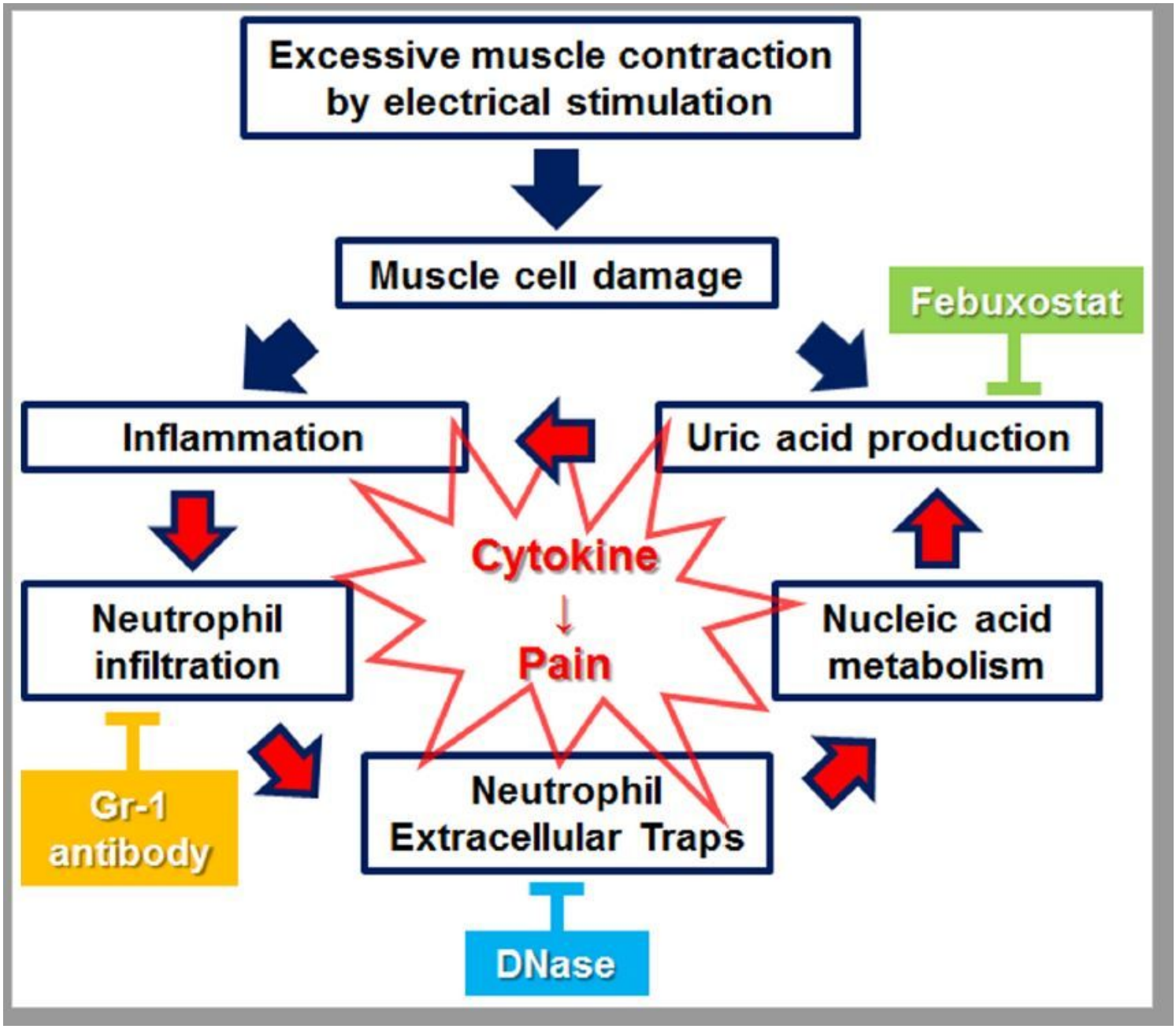

Figure 7

A simple schema of the developing pathway of muscle hyperalgesia caused by a higher tissue uric acid level in the mouse model, and the effects of inhibitors at each factor.

Supplementary Files

This is a list of supplementary files associated with this preprint. Click to download.

- Supplementalmovie1acont.mpg
- Supplementalmovie1bstimulated.mpg